

Chapter 5

Stochastic partial differential equations in Neurobiology: linear and nonlinear models for spiking neurons

Henry C. Tuckwell

Abstract Stochastic differential equation (SDE) models of nerve cells for the most part neglect the spatial dimension. Including the latter leads to stochastic partial differential equations (SPDEs) which allow for the inclusion of important variations in the densities of ion channels. In the first part of this work, we briefly consider representations of neuronal anatomy in the context of *linear* SPDE models on line segments with one and two components. Such models are reviewed and analytical methods illustrated for finding solutions as series of Ornstein-Uhlenbeck processes. However, only nonlinear models exhibit natural spike thresholds and admit traveling wave solutions, so the rest of the article is concerned with spatial versions of the two most studied nonlinear models, the Hodgkin-Huxley system and the FitzHugh-Nagumo approximation. The ion currents underlying neuronal spiking are first discussed and a general nonlinear SPDE model is presented. Guided by recent results for noise-induced inhibition of spiking in the corresponding system of ordinary differential equations, in the spatial Hodgkin-Huxley model, excitation is applied over a small region and the spiking activity observed as a function of mean stimulus strength with a view to finding the critical values for repetitive firing. During spiking near those critical values, noise of increasing amplitudes is applied over the whole neuron and over restricted regions. Minima have been found in the spike counts which parallel results for the point model and which have been termed inverse stochastic resonance. A stochastic FitzHugh-Nagumo system is also described and results given for the probability of transmission along a neuron in the presence of noise.

Henry C. Tuckwell
Max Planck Institute for Mathematics in the Sciences, Inselstr. 22, Leipzig, 04103 Germany, e-mail: tuckwell@mis.mpg.de

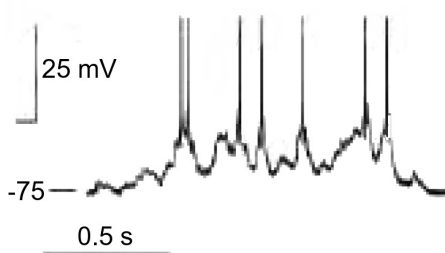
5.1 Introduction

Fundamental observations on neurons include factors which determine their spiking behaviour which is usually related to information processing in the nervous system. The need for stochastic, as opposed to deterministic, modeling in neurobiology arose from several fundamental experimental observations, between the years 1946 and 1976, of the activity of diverse nerve-cell or nerve-cell-related systems. Neurons usually emit spikes or action potentials when they receive sufficient excitatory stimuli in a sufficiently short time interval - an example of neuronal spiking is shown in Figure 1. Early observations included variability in the time-intervals between neuronal spikes (the ISI or interspike interval), random postsynaptic potentials at neuromuscular junction, the opening and closing of single ion channels and random fluctuations in electroencephalographic recordings - see [21, 43] for historical references.

The first appearance of classical random walk theory and Brownian motion in neuronal modeling came in Gerstein and Mandelbrot's pioneering work [10]. This was soon followed by the introduction of the Ornstein-Uhlenbeck process as a neuronal model [11], for which the aspects of the first-passage time problem, relevant to neuronal spiking, were solved by [32]. From that time on the primary focus has been on models of neuronal activity where the whole neuronal anatomy, including soma, dendrites and axon, is collapsed into a single point, so to speak. It is surprising that this approximation has been pursued for so long although it has often succeeded in predicting neuronal responses with considerable accuracy. However, the reason for the persistent use of point models has probably been the additional mathematical complexities involved in partial differential equations (PDEs) compared to ordinary differential equations (ODEs). See Chapter 4 for a review of single point neuronal models.

The deterministic spatial Hodgkin-Huxley (HH) system, consisting of the cable PDE and three auxiliary differential equations is one of the most successful mathematical models in physiology. In reality, linear stochastic cable models are not much more complicated than the corresponding point models. Indeed, if solutions are found by simulation, the same could be said of nonlinear models such as that of

Fig. 5.1 Action potentials recorded intracellularly from a neuron in the prefrontal cortex of rat under local electrical stimulation. Adapted from [53]. Note that spikes appear at an approximate threshold voltage of -62 mV.



HH, although more computing time is required. The main advantage of the spatial models is that more realistic distributions of ion channels, including those related to synaptic input, may be incorporated. Distinguishing locations for various ion channel types has important consequences. For example, in serotonergic neurons, low-threshold calcium current channels are thought to be mainly somatic, whereas high threshold calcium channels, which in turn activate calcium-gated potassium conductance, occur mainly on dendrites [3]. Neurons, especially those in the mammalian central nervous system, often receive many thousands of synaptic inputs from many different sources and each source has a different spatial distribution pattern [29, 52]. On the other hand, the disadvantage of spatial models is that a knowledge of many more parameters is required, many of which can at best only be approximately estimated.

5.2 Linear SPDE neuronal models: a brief summary

A general linear PDE model for nerve membrane potential, called a cable equation, takes the form

$$c_m \frac{\partial V}{\partial t} = \frac{1}{r_i} \frac{\partial^2 V}{\partial x^2} - \frac{V}{r_m} + I(x,t), \quad 0 < x < l, \quad t > 0, \quad (5.1)$$

where the symbols and their units are as follows:

x = distance from left-hand end point in cm
 t = time in seconds
 $V(x,t)$ = depolarization from rest at (x,t) in volts
 l = length of cable in cm
 r_i = resistance per unit length of internal medium (cytoplasm) in ohms/cm
 r_m = membrane resistance of unit length times unit length in ohms cm
 c_m = membrane capacitance per unit length in farads/cm
 $I = I(x,t)$ = applied current density in amperes/cm.

However, it is simpler mathematically to use units of time and space called the membrane time constant $\tau_m = c_m r_m$ and characteristic length $\lambda = (r_m/r_i)^{1/2}$ respectively, so that the above equation becomes, still using x, t for space, time variables (see Section 4.4 of [41] which also contains historical references)

$$\frac{\partial V}{\partial t} = \frac{\partial^2 V}{\partial x^2} - V + \frac{I(x,t)}{c_m^*}, \quad 0 < x < L, \quad t > 0, \quad (5.2)$$

where V is in volts and $c_m^* = \lambda c_m$ is the capacitance in farads of a characteristic length. Note that with this scaling time and space variables are dimensionless. $L = l/\lambda$ is called the electrotonic length of the cable and now the units for I are coulombs. Usually the constant c_m^* is set at unity as it simply scales the input and as the system is linear, similarly scales the response. The interval of definition as well as boundary and initial conditions are naturally required to determine specific solutions.

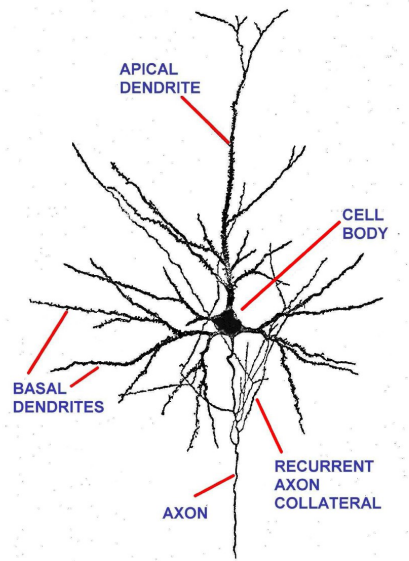
5.2.1 Geometrical or anatomical considerations

Most neurons consist of a cell body or soma (cell body), dendritic tree(s) and axon, which usually also branches prolifically. These structures are illustrated in Figure 2, which is a depiction of a pyramidal cell of rat sensorimotor cortex.

There is a great variety of sizes and forms of neurons. Most neurons in the mammalian brain are classified as excitatory or inhibitory and the majority of the former are pyramidal cells, of which there are many forms - see [16] and the review of [35]. A review of inhibitory cell types can be found in [27].

The soma is pivotal in the sense that it is, roughly speaking, the part of the cell that separates the input and output components. Many somas, however, are sites of synaptic input. Spikes which are transmitted along an axon usually emanate from, near, or at the soma.

Fig. 5.2 Showing the anatomy of a pyramidal cell from rat cerebral cortex. Adapted from [33]. The cell body (soma) has a diameter of about $20 \mu\text{m}$.

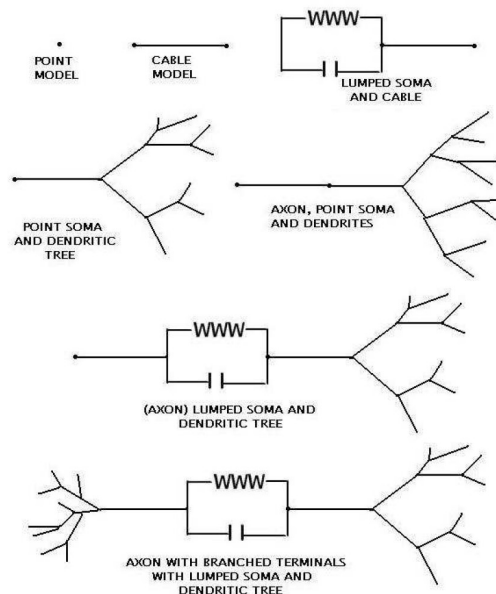


There are 9 basic geometrical and biophysical configurations which may be employed to roughly represent a neuron's anatomy for modeling with differential equations. Many of these are sketched in Figure 3.

- (i) *A single point.* Somewhat surprisingly, this, which is equivalent to space-clamping, is the most frequent representation of a neuron's geometry! ODEs are employed, but despite the simplicity, predicting details of neuronal spiking analytically is difficult. The popular model involving an Ornstein-Uhlenbeck process is still an active area in theoretical neurobiology [5, 6, 54].
- (ii) *A single line segment.* Assuming cylindrical symmetry, the line segment represents a nerve cylinder, which may be an axon or an isolated dendritic segment, or part thereof. This is probably quite accurate for such preparations as the squid axon. At one end, a point soma can, as a crude approximation, be represented with a sealed-end condition.
- (iii) *Line segment plus lumped soma.* A soma is often represented by a resistance R_s and capacitance C_s in parallel which are attached to the dendritic compartment. Such a soma circuit is referred to as a lumped (point) soma.

The remaining 6 configurations are (iv) no axon, point soma and dendritic tree, (v) no axon, lumped soma and dendritic tree, (vi) simple axon, point soma and dendritic tree, (vii) simple axon, lumped soma and dendritic tree, (viii) branched axon, point soma and dendritic tree, and lastly (ix) branched axon, lumped soma and dendritic tree(s). The last configuration contains the most anatomical and biophysical reality but is hampered by a large number of constraints.

Fig. 5.3 Several of the geometrical forms for representing nerve cells.



5.2.1.1 Reduction to a 1-dimensional cable

If, as is most often the case, a neuron has many dendritic trunks and an axon, each of which branches many times, then there are three methods of handling the geometrical (anatomical) details.

- (i) Use a cable equation for each segment.
- (ii) Assume little spatial variation of potential etc. over each segment and use an ODE for electrical potential on each segment. This is the approach used by many software packages.
- (iii) Use a mapping from the neuronal branching structure to a cylinder and thus reduce the multi-segment problem to that of a single segment, giving a cable equation in one space dimension. Most modeling studies ignore spatial extent altogether and the many of those that include spatial extent do not include a soma and hardly ever an axon. The reason is of course that the inclusion of all three major neuronal components, soma, axon and dendrites, makes for a complicated system of equations and boundary conditions.

5.2.2 Simple linear SPDE models

Many versions of the input current density $I(x, t)$ in the form of random processes were summarized in Ch. 9 of [42]. For discrete inputs of strengths a_i at space points $x_i, i = 1, \dots, n$, arriving at the times of events in the counting processes N_i , we have

$$I_1(x, t) = \sum_{i=1}^n \delta(x - x_i) a_i \frac{dN_i}{dt} \quad (5.3)$$

where $\delta(\cdot)$ is Dirac's delta function, $a_i > 0$ for an excitatory input and $a_i < 0$ for an inhibitory input. More commonly, when the N_i 's are Poisson processes, then, if the $|a_i|$'s are small enough and the associated frequencies λ_i are large enough, then a diffusion approximation (with no implied limiting procedure) may be employed so

$$I_2(x, t) = \sum_{i=1}^n \delta(x - x_i) \left(a_i \lambda_i + \sqrt{\lambda_i a_i^2} \frac{dW_i}{dt} \right) \quad (5.4)$$

where the W_i 's are standard Wiener processes, such that $W(t)$ has mean 0 and variance t , see Chapter 2. To simplify, the Poisson processes in (3) and corresponding Wiener processes in (4) are assumed to be independent. With the forms I_1 or I_2 for the current density, the SPDE, in conjunction with a threshold condition for firing, is the *spatial version of the commonly used stochastic leaky integrate and fire models*. The method of separation of variables can be used on finite intervals (e.g. $[0, L]$) to obtain an infinite series representation for V . Let the Greens function for the cable equation with given boundary conditions be

$$G(x, y; t) = \sum_k \phi_k(x) \phi_k(y) e^{-\mu_k^2 t} \quad (5.5)$$

where $\{\phi_k\}$ are spatial eigenfunctions and $\{\mu_k\}$ are the corresponding eigenvalues. Then, for example, the solution of the cable equation with multiple white noise inputs can be written

$$V(x, t) = \sum_{i=1}^n \sum_k V_{ki}(t) \phi_k(x) \quad (5.6)$$

where for each k and i

$$dV_{ki} = -[\mu_k^2 V_{ki} + a_i \lambda_i \phi_k(x_i)] dt + \sqrt{\lambda_i a_i^2} dW_i. \quad (5.7)$$

That is, each process V_{ki} is an Ornstein-Uhlenbeck process, those carrying different i indices being statistically independent. Moments of V can be readily determined analytically and simulation is a useful method for estimating firing times. Simulation methods for these systems was given in [43, 51].

5.2.2.1 Commonly employed boundary conditions

For cables on $[0, L]$ there are two simple sets of boundary conditions usually considered. Firstly, the cable may be assumed to have *sealed ends* so that

$$V_x(0, t) = V_x(L, t) = 0, \quad (5.8)$$

where subscripts denote partial differentiation. The remaining case of interest is that of *killed ends*

$$V(0, t) = V(L, t) = 0. \quad (5.9)$$

For sealed ends the eigenvalues are

$$\lambda_n = 1 + n^2 \pi^2 / L^2, n = 0, 1, \dots \quad (5.10)$$

and the normalized (to unity) eigenfunctions are $\phi_0(x) = \frac{1}{\sqrt{L}}$ and

$$\phi_n(x) = \sqrt{2/L} \cos(n\pi x/L), n = 1, 2, \dots \quad (5.11)$$

In the killed ends case, the eigenvalues are

$$\lambda_n = 1 + n^2 \pi^2 / L^2, n = 1, 2, \dots \quad (5.12)$$

and the normalized eigenfunctions are

$$\phi_n(x) = \sqrt{2/L} \sin(n\pi x/L), n = 1, 2, \dots \quad (5.13)$$

5.2.2.2 Inclusion of synaptic reversal potentials

In the above model the response to an excitation or inhibition is always of the same magnitude, regardless of the potential when the input arrives. In reality, since synaptic potentials are generated by ion currents whose components have specific Nernst potentials, the response to a synaptic input depends on the prior potential. This aspect was introduced in point models by [38] for the Poisson case and for the diffusion approximation by [15]. Inclusion of reversal potentials in the cable model gives the following SPDE for n_E excitatory inputs at the space points $x_{E,j}$ arriving at the event times of $N_{E,j}$ and n_I inhibitory inputs at the points $x_{I,k}$ at the times of events in $N_{I,k}$

$$\begin{aligned} \frac{\partial V}{\partial t} = & \frac{\partial^2 V}{\partial x^2} - V + \sum_{j=1}^{n_E} a_{E,j} \delta(x - x_{E,j}) (V - V_E) \frac{dN_{E,j}}{dt} \\ & - \sum_{k=1}^{n_I} a_{I,k} \delta(x - x_{I,k}) (V - V_I) \frac{dN_{I,k}}{dt}. \end{aligned} \quad (5.14)$$

Here the quantities $a_{E,j} > 0$ and $a_{I,k} > 0$ determine the magnitudes of the responses to synaptic inputs. It is assumed that all excitatory inputs have the reversal potential V_E and all inhibitory inputs have reversal potential V_I , though this is a simplification. If the processes $N_{E,j}$ and $N_{I,k}$ have mean rates $\lambda_{E,j}$ and $\lambda_{I,k}$, respectively, and are independent, then a diffusion approximation can be constructed with the SPDE

$$\begin{aligned} \frac{\partial V}{\partial t} = & \frac{\partial^2 V}{\partial x^2} - V + \sum_{j=1}^{n_E} a_{E,j} \lambda_{E,j} \delta(x - x_{E,j}) (V - V_E) \\ & + \sum_{j=1}^{n_E} \delta(x - x_{E,j}) \sqrt{a_{E,j}^2 \lambda_{E,j} (V - V_E)^2} \frac{dW_{E,j}}{dt} \\ & - \sum_{k=1}^{n_I} a_{I,k} \lambda_{I,k} \delta(x - x_{I,k}) (V - V_I) \\ & + \sum_{k=1}^{n_I} \delta(x - x_{I,k}) \sqrt{a_{I,k}^2 \lambda_{I,k} (V - V_I)^2} \frac{dW_{I,k}}{dt} \end{aligned} \quad (5.15)$$

where the $W_{E,j}$ and $W_{I,k}$ are (possibly) independent standard Wiener processes. Both the discontinuous model and its diffusion approximation will be the subject of future investigations.

5.2.2.3 Two-parameter white noise input

Of interest is the case of uniform two-parameter white noise $w(x,t)$ so that

$$I_3(x,t) = a + bw(x,t), \quad (5.16)$$

where $\{w(x,t), x \in [0, L], t \geq 0\}$ is a space-time white noise with covariance function

$$\text{Cov}[w(x,s), w(y,t)] = \delta(x-y)\delta(s-t). \quad (5.17)$$

The solution has the decomposition

$$V(x,t) = \sum_k V_k(t)\phi_k(x) \quad (5.18)$$

which involves Ornstein-Uhlenbeck processes which are all statistically independent, satisfying the SDEs

$$dV_k = [a_k - \mu_k^2 V_k] dt + b dW_k, \quad (5.19)$$

where

$$a_k = a \int_0^L \phi_k(y) dy \quad (5.20)$$

and the one-parameter Wiener processes are defined by

$$W_k(t) = \int_0^L \int_0^t \phi_k(y) w(y,s) ds dy. \quad (5.21)$$

Analytical and simulation approaches for finding the statistical properties of V and firing times were reported in [49].

5.2.2.4 Synaptic input as a mixture of jump and diffusion processes

For many neurons, some excitatory postsynaptic potentials have large amplitudes, of order a few to several millivolts, whereas others may be much smaller. Under these conditions a model may be constructed in which some inputs are represented by discontinuous (jump) processes which are not well approximated by diffusions whereas smaller amplitude inputs are amenable to such approximations. This aspect was introduced in point models by [39]. Inclusion in the spatial model with reversal potentials is immediate by taking linear combinations of input terms from the jump and diffusion cases as follows

$$\begin{aligned}
\frac{\partial V}{\partial t} = & \frac{\partial^2 V}{\partial x^2} - V + \sum_{j=1}^{n_E} a_{E,j} \delta(x - x_{E,j}) (V - V_E) \frac{dN_{E,j}}{dt} \\
& - \sum_{k=1}^{n_I} a_{I,k} \delta(x - x_{I,k}) (V - V_I) \frac{dN_{I,k}}{dt} \\
& + \sum_{j=1}^{n'_E} a'_{E,j} \lambda'_{E,j} \delta(x - x'_{E,j}) (V - V_E) \\
& + \sum_{j=1}^{n'_E} \delta(x - x'_{E,j}) \sqrt{a'^2_{E,j} \lambda'_{E,j} (V - V_E)^2} \frac{dW'_{E,j}}{dt} \\
& - \sum_{k=1}^{n'_I} a'_{I,k} \lambda'_{I,k} \delta(x - x'_{I,k}) (V - V_I) \\
& + \sum_{k=1}^{n'_I} \delta(x - x'_{I,k}) \sqrt{a'^2_{I,k} \lambda'_{I,k} (V - V_I)^2} \frac{dW'_{I,k}}{dt}, \quad (5.22)
\end{aligned}$$

where unprimed quantities refer to the large amplitude inputs and the primed quantities to those for which a diffusion approximation can be made.

5.2.3 Two-component linear SPDE systems

The above SPDE containing derivatives of counting processes, such as Poisson processes, has solutions with discontinuities due to the impulsive nature of the derivatives dN_i/dt . In real neurons the arrival of, for example, an excitatory synaptic potential is signalled by a rapid but smooth increase in membrane potential, followed by an approximately exponential decay. In order to give a more realistic representation, the time derivative of the current density is set to

$$\frac{\partial I}{\partial t} = -\alpha I + a_E \frac{\partial^2 N_E}{\partial x \partial t} - a_I \frac{\partial^2 N_I}{\partial x \partial t}, \quad (5.23)$$

where N_E and N_I are two-parameter counting processes (e.g. Poisson processes), not necessarily independent, so that I has discontinuities but V itself is smooth (continuous). Here $a_E, a_I \geq 0$. In real neurons, rates and amplitudes will, naturally, vary in space and time and amplitudes may be random. However, for simplicity it is assumed that all excitatory events cause I to increase locally by a_E and all inhibitory events result in a jump down in I of magnitude a_I . The rates may also be assumed constant so that λ_E and λ_I are the mean number of excitatory and inhibitory events, respectively, per unit area in the (x, t) -plane. Because the system is linear and homogeneous, the statistical properties are relatively straightforward to determine analytically. A simpler model with an Ornstein-Uhlenbeck current at a point was analyzed in [50].

Put $K = a_E \lambda_E - a_I \lambda_I$ which is mean net synaptic drive. With *sealed ends* it is readily shown that the mean depolarization is

$$E[V(x,t)] = \frac{K}{\alpha} \left[1 - e^{-t} + \frac{1}{1-\alpha} (e^{-t} - e^{-\alpha t}) \right], \quad \alpha \neq 1. \quad (5.24)$$

This is the same as the result for the infinite cable, giving a mean which is independent of position. In the case of *killed ends* the mean voltage along the cable is given by

$$E[V(x,t)] = \frac{4K}{\alpha\pi} \sum_{n=1}^{\infty} \frac{\sin(n\pi x/L)}{n} \left\{ \frac{1 - e^{-\lambda_n t}}{\lambda_n} - \frac{(e^{-\alpha t} - e^{-\lambda_n t})}{\lambda_n - \alpha} \right\}, \quad (5.25)$$

where summation is over odd values of n only.

A diffusion approximation may be employed here so that, assuming the postsynaptic potential amplitudes and the rates are constant

$$\frac{\partial I}{\partial t} = -\alpha I + K + \kappa w(x,t) \quad (5.26)$$

where $\kappa = \sqrt{a_E^2 \lambda_E + a_I^2 \lambda_I}$. Many statistical properties of the corresponding membrane potential V were obtained and the effects of various spatial distributions of synaptic input, based on data for cortical pyramidal cells, were found on the interspike interval distribution [44, 45]. With excitation only, the ISI distribution is unimodal with a decaying exponential appearance and with a large coefficient of variation. As inhibition near the soma grows, two striking effects emerge. The ISI distribution shifts first to bimodal and then to unimodal with an approximately Gaussian shape with a concentration at large intervals. At the same time the coefficient of variation of the ISI drops dramatically to less than 1/5 of its value without inhibition.

5.3 Nonlinear models for spiking neurons

In 1952 Hodgkin and Huxley set forth a dynamical system of PDEs to describe action potential generation and propagation in the squid giant axon. From the time of that original work to the present day, their method of dividing the membrane current into a capacitive and ionic component has provided the basis for mathematical models of many nerve cells, as exemplified recently by spatial models of thalamic pacemaker cells [31], and paraventricular neurons [22]. The capacitive component of the current is always assumed to have the simple form $C \frac{\partial V}{\partial t}$. The main principle that emerges from all these works is that to quantify the ionic components, each ion-channel type is represented by an activation variable m and, if appropriate, an inactivation variable h . The current density for each channel usually has the form $J = g_{max} m^m h (V - V_i)$ where g_{max} , which may depend on position, is the conductance

available with all channels open, although sometimes the constant field form is more accurate [4]. An important effect is the modulation of conductances by various biochemical mechanisms [23].

5.3.1 *The ionic currents underlying neuronal spiking*

The original HH-system for squid contained only sodium, potassium and leak currents so that the total ionic current was

$$I_{ion} = I_{Na} + I_K + I_{leak} \quad (5.27)$$

Furthermore, in squid axon the distribution of the corresponding ion channels was assumed to be spatially uniform. Models of motoneurons [7, 36] and cortical pyramidal cells [19, 26] have also contained only these three components, but with varying channel densities over the neurons surface. However, in the last three decades it has become apparent that one needs to consider many ion channels apart from the original sodium and potassium channels in the HH-model. For example, it is now known that calcium currents are important in the spiking activity of most, if not all, CNS neurons [21, 37]. Calcium currents, which are themselves voltage-gated, do not only contribute directly to membrane currents, but also cause increases in intracellular calcium concentration. Such inward currents cause changes in calcium concentration-dependent conductances of which an important example is the calcium-activated potassium current I_{KCa} . To describe nerve cell activity with a degree of biophysical reality it is therefore frequently essential to take into account calcium dynamics. The latter entails buffering, sequestration, diffusion and pumping or active transport; see for example [4]. Unfortunately from the point of view of mathematical modeling, the number of ion-channel types is enormous, there being 10 types of calcium channel (with many subtypes) [8] and 40 types of potassium channel [14]. By 1997 there had been at least 40 types of ion channel found just in nerve terminals [30]. See [25] for an earlier yet classic summary of channel types in various mammalian nerve cells.

5.3.2 *A general SPDE for nerve membrane potential*

A general HH-type electrophysiological model with the addition of synaptic and applied inputs in the form of an SPDE for the membrane potential $V(x, t)$ on a segment of a nerve can be described in one space dimension, assuming approximately cylindrical geometry. In most cases a neuronal cell body with dendritic trees and an axon will be represented by a collection of such segments and sometimes a special (probably ODE) equation for the somatic component. Thus, in the case of a real neuron, many boundary conditions will need to be satisfied. Including only purely voltage-

dependent channels, on each segment we have

$$\frac{\partial V}{\partial t} = \frac{\partial^2 V}{\partial x^2} + \sum_{i=1}^n g_{i,max} m_i^{p_i} h_i^{q_i} (V - V_i) + I_{syn} + I_{app} \quad (5.28)$$

$$\frac{\partial m_i}{\partial t} = \alpha_{m_i}(V)(1 - m_i) - \beta_{m_i}(V)m_i \quad (5.29)$$

$$\frac{\partial h_i}{\partial t} = \alpha_{h_i}(V)(1 - h_i) - \beta_{h_i}(V)h_i \quad (5.30)$$

$$I_{syn} = \sum_k a_k \delta(x - x_k)(V - V_k^*) \frac{dN_k}{dt} \quad (5.31)$$

where there are n distinct types of ion channel. Here I_{syn} is synaptic input occurring at space points x_k with reversal potentials V_k^* and amplitudes a_k according to the point processes N_k , and I_{app} is any experimentally applied current. The i -th channel type has maximal conductance density $g_{i,max}$ and the corresponding activation and inactivation variables are m_i and h_i , respectively. If there is no inactivation, as is often the case, such as for some high voltage threshold calcium channels and the potassium direct-rectifier channels, then q_i can be set at zero. For a leak current, which may have more than one component, both p_i and q_i can be set to zero. The maximal conductances and the synaptic and applied currents are space- and possibly time-dependent. Calcium-dependence has been omitted because of the complication that some calcium currents and not others are involved in the activation of, for example, potassium channels. Calcium dynamics has been taken into account in many different ways, even for the same neuron type [28, 31]. To illustrate, the L-type calcium channel has calcium-dependent inactivation so if the internal calcium concentration is Ca_i , the external calcium concentration is Ca_o , then all deterministic formulations of the L-type calcium current employed in modeling to date are included in the general form

$$I_{CaL} = m^{p_1}(V,t)h^{p_2}(V,t)f(Ca_i,t)F(V,Ca_i,Ca_o), \quad (5.32)$$

where $m(V,t)$ is the voltage-dependent activation variable, $h(V,t)$ is the voltage-dependent inactivation variable and $f(Ca_i,t)$ is the (internal) calcium-dependent inactivation variable. The factor F contains membrane biophysical parameters and is either of the Ohmic form used in the original HH model, or the constant-field form, often called the Goldman-Hodgkin-Katz form [42].

5.4 Stochastic spatial Hodgkin-Huxley model

Recent studies of the HH-system of ODEs with stochastic input have revealed interesting phenomena which have a character opposite to that of stochastic resonance. In the latter, there is a noise level at which some response variable achieves a maximum. In particular, at mean input current densities near the critical value (about 6.4

$\mu A/cm^2$) for repetitive firing, it was found that noise could strongly inhibit spiking. Furthermore, there occurred, for given mean current densities, a minimum in the firing rate as the noise level increased from zero [48]. It is of interest to see if these phenomena extend to the spatial HH-system which we describe forthwith. Historically, a study of the properties of the output spike train of an HH cable with Poisson inputs was previously described by [12] and simulations of random channel openings were considered by [34].

The following system of differential equations was proposed [17] to describe the evolution in time and space of the depolarization V in the squid giant axon:

$$C_m \frac{\partial V}{\partial t} = \frac{a}{2R_i} \frac{\partial^2 V}{\partial x^2} + \bar{g}_K n^4 (V_K - V) + \bar{g}_{Na} m^3 h (V_{Na} - V) + g_l (V_l - V) + I(x, t) \quad (5.33)$$

$$\frac{\partial h}{\partial t} = \alpha_h(V)(1 - h) - \beta_h(V)h \quad (5.34)$$

$$\frac{\partial m}{\partial t} = \alpha_m(V)(1 - m) - \beta_m(V)m \quad (5.35)$$

$$\frac{\partial n}{\partial t} = \alpha_n(V)(1 - n) - \beta_n(V)n. \quad (5.36)$$

Here $C_m, \bar{g}_K, \bar{g}_{Na}, g_l$, and $I(x, t)$ are respectively the membrane capacitance, maximal potassium conductance, maximal sodium conductance, leak conductance and applied current density for unit area (1sq cm). R_i is the intracellular resistivity and a is the fiber radius. n, m and h are the potassium activation, sodium activation and sodium inactivation variables and their evolution is determined by the voltage-dependent coefficients

$$\alpha_n(V) = \frac{10 - V}{100[e^{(10-V)/10} - 1]}, \quad \beta_n(V) = \frac{1}{8}e^{-V/80} \quad (5.37)$$

$$\alpha_m(V) = \frac{25V}{10[e^{(25-V)/10} - 1]}, \quad \beta_m(V) = 4e^{-V/18} \quad (5.38)$$

$$\alpha_h(V) = \frac{1}{100}e^{-V/20}, \quad \beta_h(V) = \frac{1}{e^{(30-V)/10} + 1} \quad (5.39)$$

The following standard parameter values are employed: $a = 0.0238, R_i = 34.5, C_m = 1, \bar{g}_K = 36, \bar{g}_{Na} = 120, g_l = 0.3, V_K = 12, V_{Na} = 115$ and $V_l = 10$. For the initial values, $V(0) = 0$ and for the auxiliary variables the equilibrium values are used, for example $n(0) = \frac{\alpha_n(0)}{\alpha_n(0) + \beta_n(0)}$. The units for these various quantities are as follows: all times are in msec, all voltages are in mV, all conductances per unit area are in mS/cm^2 , R_i is in ohm-cm, C_m is in $\mu F/cm^2$, distances are in cm, and current density is in microamperes/cm².

Note that with the standard parameters, the HH-model does not act as a spontaneous pacemaker. One may turn the HH neuron into a spontaneously firing cell by shifting, for example, the half activation potential to -30.5 mV from about -28.4 mV (assumed resting at -55 mV) whereupon there is a threshold for repetitive spik-

ing around +1.8 nA (hyperpolarizing). Then for the HH system of ODEs, similar phenomena, including inverse stochastic resonance, are found with noise as with the standard parameter set. This robustness is expected to apply also to the spatial model as discussed below.

5.4.1 Noise-free excitation

We firstly consider the HH-system with a constant input current over a small interval so that $I(x,t) = \mu(x,t)$ where

$$\mu(x,t) = \mu > 0, \quad 0 \leq x \leq x_1 \leq L, \quad t > 0, \quad (5.40)$$

and zero current density elsewhere. The initial condition for V is resting level and the auxiliary variables have their corresponding equilibrium values. The length was set at $L = 6$ cm. With $x_1 = 0.2$ the response for $\mu = 4$ is a solitary spike. With $\mu = 6$ a doublet of spikes propagates along the nerve cylinder and beyond some critical value of μ there ensues a train of regularly spaced spikes, as for example with $\mu = 7.5$.

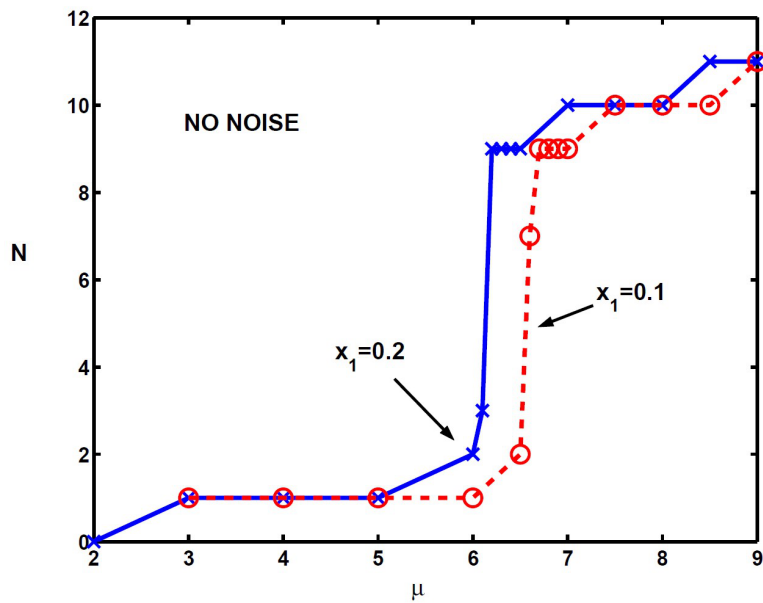


Fig. 5.4 The number of spikes N on $(0, L)$ at $t = 160$ is plotted against the level of excitation μ in the absence of noise. The dashed curve is for the smaller region of excitation to $x_1 = 0.1$ whereas the solid curve is for $x_1 = 0.2$. Notice the abrupt increases in spike rates at values close to the bifurcation to repetitive firing, being about 6.1 for $x_1 = 0.2$ and 6.5 for $x_1 = 0.1$.

The latter case corresponds to repetitive and periodic firing in the HH-system of ODEs. In order to quantify the spiking activity, the maximum number N of spikes on (0,6) is found and figure 5.4 shows the dependence of N on the mean input current density, μ , for two values of $x_1 = 0.1$ and $x_1 = 0.2$. For $\mu < 2$ no spikes occurred for both values of x_1 . A solitary spike emerged for $\mu \geq 2$ and when μ reached 6 in the case of $x_1 = 0.2$ and 6.5 in the case of $x_1 = 0.1$, a doublet arose and propagated along the cylinder. For slightly greater values of μ , an abrupt increase in the number of spikes, indicating that a bifurcation had occurred (see [48] for an explanation of such phenomena). Subsequently the number of spikes reached a plateau and when μ reached 9, the largest value considered here, the number of spikes was 11 for both values of x_1 . In consideration of the behavior of the HH system of ODEs with noise, it was then of interest to examine the effects of noise on the spike counts near the bifurcation point for the PDE case.

5.4.2 Stochastic stimulation

The HH-system of PDEs was therefore considered with applied currents of the following form

$$I(x,t) = \mu(x,t) + \sigma(x,t)w(x,t) \quad (5.41)$$

on a cylindrical nerve cell extending from $x = 0$ to $x = L$, where $\mu(x,t)$ is as above and for the random component

$$\sigma(x,t) = \sigma > 0, \quad 0 \leq x_2 \leq x \leq x_3 \leq L, \quad t > 0, \quad (5.42)$$

and zero elsewhere. Here $\{w(x,t), x \in [0,L], t \geq 0\}$ is a two-parameter white noise with covariance function

$$\text{Cov}[w(x,s), w(y,t)] = \delta(x-y)\delta(t-s), \quad (5.43)$$

$\mu(x,t)$ and $\sigma(x,t)$ being deterministic functions specifying the mean and variance of the noisy input. The numerical integration of the resulting stochastic HH system of PDEs is performed by discretization using an explicit method whose accuracy has been verified by comparison with analytical results in similar systems [45], there being no available analytical results for the HH model.

Figure 5.5 shows examples of the effects of noise with the following parameters: $\mu = 6.7$, $x_1 = 0.1$, $x_2 = 0$, and $x_3 = L = 6$. The records show the membrane potential as a function of x at $t = 160$. In the top record there is no noise and there are 9 spikes. In the middle two records, with a noise level of $\sigma = 0.1$ there is a significant diminution of the spiking activity, with only 1 spike in one case and 3 in the other. With the noise turned up to $\sigma = 0.3$ (bottom record) the number of spikes is greater, there being 6 in the example shown.

With $x_1 = 0.1$, mean spike counts were obtained at various σ for $\mu = 5, 6.7$ and 7. The first of these values is less than the critical value for repetitive firing (see fig-

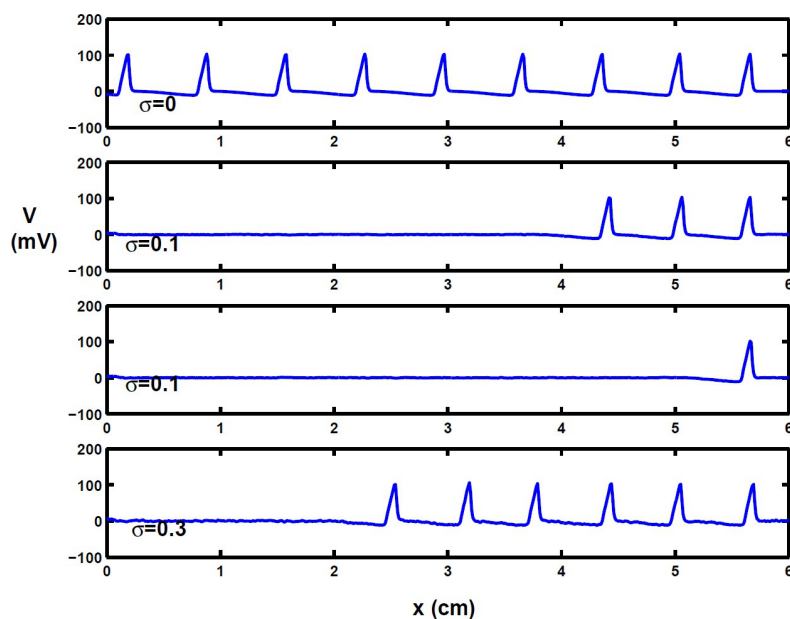


Fig. 5.5 Showing the effects of noise on spiking for mean current densities near the bifurcation to repetitive spiking. Parameters are $\mu = 6.7$, $x_1 = 0.1$, $x_2 = 0$, and $x_3 = L = 6$. In the top record with no noise there is repetitive firing which, as shown in the second and third records, is strongly inhibited by a relatively small noise of amplitude $\sigma = 0.1$. A larger noise amplitude $\sigma = 0.3$ leads to much less inhibition.

ure 5.4) and the other two close to and just above the critical value. Relatively small numbers of trials were performed as integration of the PDEs naturally takes much longer than the ODEs. Hence, the number of trials in the following is 25, which is a small statistical sample, but is sufficient to show the main effects. Figure 5.6 shows plots of mean spike counts, $E[N]$, as explained above, versus noise level. For $\mu = 5$, $E[N]$ increases monotonically as σ increases from 0 to 0.3. When $\mu = 6.7$, which is very close to the critical value for repetitive firing, a small amount of noise causes a substantial decrease in firing (cf figure 5.5) with the appearance of a minimum near $\sigma = 0.1$. For $\mu = 7$, where indefinite repetitive firing occurs without noise, a similar reduction in firing activity occurs at all values of σ up to the largest value employed, 0.3. Furthermore, a minimum in mean spike count also occurs near $\sigma = 0.1$, a phenomenon referred to previously as *inverse stochastic resonance* [13]. In some trials, secondary phenomena were observed as in the FitzHugh-Nagumo (FHN) system [45]. An example of what might be called an *anomalous case* occurred for $x_1 = 0.1$, with the mean excitation level $\mu = 5$ below the threshold for repetitive firing and noise of amplitude $\sigma = 0.3$ extending along the whole cable. A single spike emerges from the left hand end. By $t = 32$ a pair of spikes is seen to emerge at $x \approx 5$, one traveling towards the emerging spike and one to the right. Not

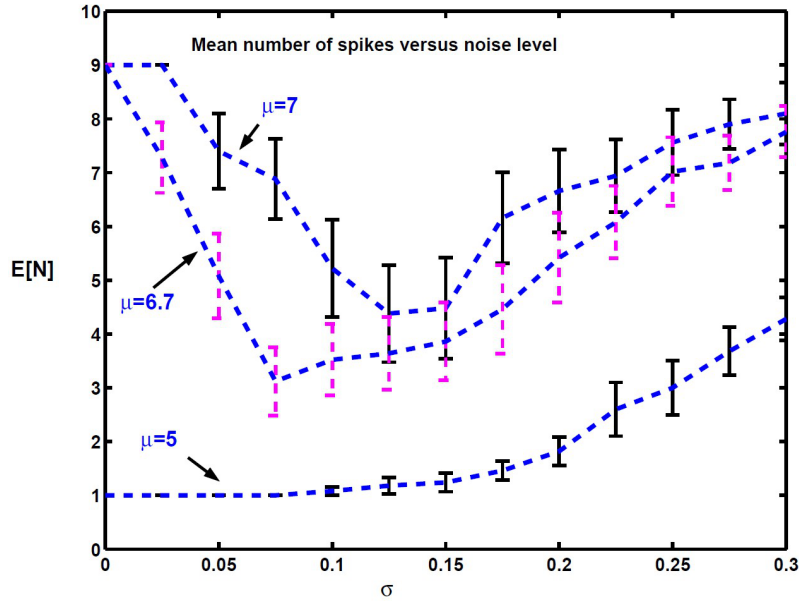


Fig. 5.6 Mean number of spikes as a function of noise level for various values of the mean level of excitation μ with excitation on $(0,0.1)$. The bottom curve is for a value of μ well below the critical value at which repetitive firing occurs. 95% confidence limits are indicated.

long after $t = 80$ the left-going secondary spike collides with the emerging right-going spike and these spikes annihilate each other. Thus, the spike count on $(0, L)$ ends up at 0 at $t = 160$ due to interference between a noise-generated spike and the spike elicited by the deterministic excitation.

With $x_1 = 0.2$, mean spike counts were similarly obtained with various noise amplitudes for $\mu = 5, 6.2$ and 6.5 . Again, the first of these values is less than the critical value for repetitive firing (see figure 5.4) and the other two close to and just above the critical value. Similar behavior in spiking activity occurred as σ varied as for $x_1 = 0.1$. Thus, these findings of inverse stochastic resonance parallel those found for the HH system of ODEs and although there is no standard bifurcation analysis for the PDE system, it is probable that most of the arguments which apply to the system of ODEs apply to the PDEs. It was also found that noise over the small region to $x = 0.05$ reduces the mean spike count by 48% and when the extent of the noise is to $x \geq 0.1$ the mean spike count drops to about one third of its value without noise. Thus, there is only a small further reduction in spiking when the noise extends to the whole interval. Similar results were obtained for $x_1 = 0.2$. Thus, noise over even a small region where the excitation occurs may inhibit partially or completely the emergence of spikes from a trigger zone just as or almost as effectively as noise along the whole extent of the neuron. Surprisingly, with $x_1 = 0.1$, $x_2 = 0.1$ and $x_3 = 0.2$ so that the small noise patch was just to the right of the

excitatory stimulus, no reduction in spike count occurred. Thus, noise at the site of the excitation causes a significant reduction in spike count, but noise with the same magnitude and extent but disjoint from the region of excitation has, at least in the cases examined, no effect. However, a small amount of interference with the outgoing spike train did occur when the noise amplitude was stronger at $\sigma = 0.3$ with $x_1 = 0.1$ and the noise was on $(0.1, 0.2)$. Such interference is probably due to a different mechanism from switching the system from one attractor (firing regularly) to another (a stable point) and possibly is due to the instigation of secondary wave phenomena as described above in the anomalous case and in the FHN system [45]. For more details of the effects of noise on the instigation and propagation of spikes in the spatial HH system, including both means and variances of spike numbers, see [46, 47].

5.5 A stochastic spatial FitzHugh-Nagumo system

The FHN system has long since been employed as a simplification of the HH model as it shares many of its properties and only has two rather than four components. Hence we here briefly discuss the FHN spatial model with noise. See also Chapter 5.6 for a different treatment of the FHN system. In one space dimension, the FHN model can be written, using subscript notation for partial differentiation,

$$u_t = D_1 u_{xx} + \kappa u(u-a)(1-u) - \lambda v + I(x,t), \quad (5.44)$$

$$v_t = D_2 v_{xx} + \varepsilon'[u - pv + b], \quad (5.45)$$

$$0 < x < L, \quad t > 0,$$

where the voltage variable is $u(x,t)$ and a recovery variable is $v(x,t)$. The quantities $\kappa, \lambda, \varepsilon, p, D_1$ and D_2 are positive and usually taken to be constants, although they could vary with both x and t . The parameter b can be positive, negative or zero. The applied current or input signal $I(x,t)$ may be due to external or intrinsic sources. In the majority of applications $D_1 = 1$ and $D_2 = 0$.

5.5.1 The effect of noise on the probability of transmission

One aspect of interest is the effects of noise on the propagation of an action potential. To this end we consider an FHN system with the original parameterization [9]

$$u_t = u_{xx} + u - \frac{u^3}{3} - v + I(x,t) \quad (5.46)$$

$$v_t = 0.08(u - 0.8v + 0.7). \quad (5.47)$$

and let

$$I(x,t) = \sigma(x)w(x,t), \quad (5.48)$$

that is, driftless white noise with amplitude which may depend on position. Sealed end conditions are employed. In order to start an action potential we apply a current J at $x = 0$ for $0 \leq t \leq t^*$. The boundary conditions are thus

$$u_x(0,t) = J, \quad 0 < t \leq t^*, \quad (5.49)$$

$$u_x(0,t) = 0, \quad t > t^*, \quad (5.50)$$

$$u_x(L,t) = 0, \quad t > 0. \quad (5.51)$$

For initial conditions for the general system of SPDEs $u_t = D_1 u_{xx} + f(u,v) + \sigma w(x,t)$ and $v_t = D_2 v_{xx} + g(u,v)$ we choose suitable equilibrium values

$$u(x,0) = u^*, \quad v(x,0) = v^*, \quad 0 < x < L, \quad (5.52)$$

where u^* and v^* satisfy

$$f(u^*, v^*) = 0, \quad g(u^*, v^*) = 0. \quad (5.53)$$

For the original FHN model, these equilibrium values are $u^* = -1.1994$ and $v^* = -0.6243$, being the unique real solution of $u - u^3/3 - v = 0$ and $0.08(u - 0.8v + 0.7) = 0$.

With this parameterization an action potential (solitary wave solution) has a speed of about 0.8 space units per time unit. If a space unit is chosen to represent 0.1 mm and a time unit is chosen as 0.04 msec, then the speed of propagation is 2 meters/sec which is close to the value for unmyelinated fibers. We set the overall length at 50 space units or 5 mm to be near the order of magnitude of real neurons. Suppose that there is a noisy background throughout the length of the nerve so that $\sigma(x) = \sigma$, a constant. Often a solitary wave passes fairly well unchanged but this may not be so even for small amplitude noise over larger distances. When $\sigma = 0.225$ or 0.25 several outcomes are possible. The wave may pass fairly well unchanged, or the wave progresses some distance but dies due to noise interference, or sometimes, as seen above in the HH model, a subsidiary noise-induced wave starts at the right hand end and propagates towards the oncoming wave induced by the end current. Annihilation of the original right-going wave occurs when it collides with the back-travelling wave and the result is a failure of propagation.

The dependence on noise amplitude of the probability of successful transmission, $p_{trans}(\sigma)$, of an action potential, instigated at $x = 0$, was investigated for both uniform noise on $(0, L)$, where $L = 5$ mm, and for noise restricted to $2.5 \leq x \leq 3.5$. The results are shown in figure 5.7 where probability of transmission is plotted against σ . The results for uniform noise (blue crosses) can be divided into two regimes, to the left and right of the point P. The rate of decline of p_{trans} as σ increases from 0.12 to about 0.26 is slower by a factor of about 4.5 than that as σ increases from 0.26 to 0.40. Examination of the sample paths showed that there are two kinds of transmission failure. One is due to purely noise interference occurring at the smaller values of σ and resulting in the annihilation of the traveling wave.

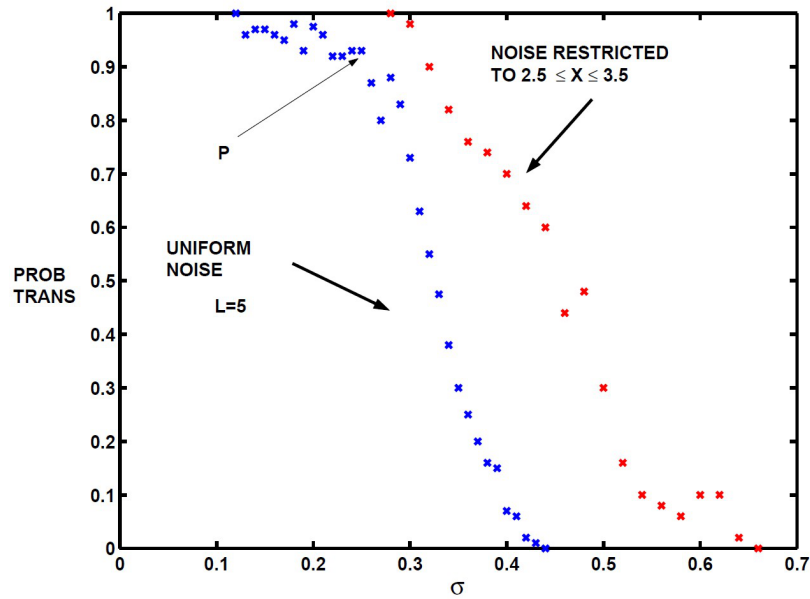


Fig. 5.7 The probability of transmission of the action potential versus noise amplitude. Blue crosses are for uniform noise whereas red crosses are for the case of noise restricted to a small region based on 100 trials per point. The point P demarcates for the uniform case the regime for smaller σ where the noise essentially annihilates the oncoming wave from the regime for larger σ where the noise is sufficiently strong to give rise to non-local large often disruptive responses.

The other occurs when the noise itself starts a secondary disturbance of sufficient magnitude that it may grow into a substantial response, which may take the form of another wave or multiple waves. Sometimes the original wave almost dies and noise leads to its revival as a secondary wave. When the noise was restricted to be over a small space interval, transmission failure occurred usually by interference by noise rather than secondary phenomena. That is, the original travelling wave found it difficult to traverse the noisy patch. See [45] for further results and discussion.

5.6 Discussion

We have presented several SPDE models in neurobiology, with focus on single neurons. In Chapter 6.5 SPDE models are presented for the cerebro-cortical phenomenon of spreading depression. Although the mathematics involved in establishing existence and describing properties of the solutions to such SPDEs is highly abstract [2, 20], simulation techniques, which may be explicit or implicit, enable one to determine many statistical properties relevant to electrophysiological investigations. For the HH system of PDEs, [18] undertook a study of the effects of noise

on nerve impulse propagation using one of the stochastic models proposed by [40]. In the present article, for the HH PDE model we also have focused on additive noise, but another somewhat different approach is to consider noisy ion channel dynamics, theoretically explored in [1]. Our main finding was that the phenomenon of inverse stochastic resonance, recently elaborated on for the HH system of ODEs, does occur in the HH SPDE system as well. Although noise along the whole neuron was found to suppress spiking near the critical levels of mean excitation for repetitive spiking, with a concomitant minimum as noise amplitude increased away from zero, noise over a small region near the main source of excitation was found to be nearly as potent in its inhibitory effect.

The FHN system has been employed in numerous settings [24] outside its original domain as an approximation to the HH nerve cell model. Here we have focused briefly on the effects of additive noise in the PDE version, which is elaborated on in [45]. Two modes of inhibition of transmission by noise were found, one local and the other due to secondary wave phenomena, which also occurs in the HH SPDE system.

Acknowledgements I wish to express appreciation to Professors Susanne Ditlevsen and Michael Sorensen for organizing the Middelfart meeting and Professor Jerry Batzel for his help in organizing the proceedings. I also thank Prof Dr Jürgen Jost for his fine hospitality at MIS MPI.

References

1. Austin, T.: The emergence of the deterministic Hodgkin-Huxley equations as a limit from the underlying stochastic ion-channel mechanism. *Ann. Appl. Prob.* **18**, 1279–1325 (2008)
2. Bergé, B., Chueshov, I., Vuillermot, P.A.: On the behavior of solutions to certain parabolic SPDEs driven by Wiener processes. *Stoch. Proc. Appl.* **92**, 237–263 (2001)
3. Burlhis, T., Aghajanian, G.: Pacemaker potentials of serotonergic dorsal raphe neurons: contribution of a low-threshold Ca^{2+} conductance. *Synapse* **1**, 582–588 (1987)
4. Destexhe, A., Sejnowski, O.: *Thalamocortical Assemblies*. Oxford University Press, Oxford UK (2001)
5. Ditlevsen, S., Ditlevsen, O.: Parameter estimation from observations of first-passage times of the Ornstein-Uhlenbeck process and the Feller process. *Prob. Eng. Mech.* **23**, 170–179 (2008)
6. Ditlevsen, S., Lansky, P.: Estimation of the input parameters in the Ornstein-Uhlenbeck neuronal model. *Phys. Rev. E* **71**, Art. No. 011,907 (2005)
7. Dodge, F., Cooley, J.: Action potential of the motoneuron. *IBM J Res Devel* **17**, 219–229 (1973)
8. Dolphin, A.: Calcium channel diversity: multiple roles of calcium channel subunits. *Curr Opin Neurobiol* **19**, 237–244 (2009)
9. FitzHugh, R.: *Mathematical models of excitation and propagation in nerve*. In *Biological Engineering*. McGrawHill Book Co., New York (1969)
10. Gerstein, G., Mandelbrot, B.: Random walk models for the spike activity of a single neuron. *Biophys J* **4**, 4168 (1964)
11. Gluss, B.: A model for neuron firing with exponential decay of potential resulting in diffusion equations for probability density. *Bull Math Biophysics* **29**, 233–243 (1967)
12. Goldfinger, M.: Poisson process stimulation of an excitable membrane cable model. *Biophys J* **50**, 27–40 (1986)

13. Gutkin, B., Jost, J., Tuckwell, H.: Inhibition of rhythmic neural spiking by noise: the occurrence of a minimum in activity with increasing noise. *Naturwissenschaften* **96**, 1091–1097 (2009)
14. Gutman, G., Chandy, K., Grissmer, S., Lazdunski, M., McKinnon, D., Pardo, L., Robertson, G., Rudy, B., Sanguinetti, M., Stuhmer, W., Wang, X.: International Union of Pharmacology. LIII. Nomenclature and molecular relationships of voltage-gated potassium channel. *Pharmacol Rev* **57**, 473,508 (2005)
15. Hanson, F., Tuckwell, H.: Diffusion approximations for neuronal activity including synaptic reversal potentials. *J. Theor. Neurobiol.* **2**, 127–153 (1983)
16. Hellwig, B.: A quantitative analysis of the local connectivity between pyramidal neurons in layers 2/3 of the rat visual cortex. *Biol Cybern* **82**, 111–121 (2000)
17. Hodgkin, A., Huxley, A.: A quantitative description of membrane current and its application to conduction and excitation in nerve. *J Physiol* **117**, 500–544 (1952)
18. Horikawa, Y.: Noise effects on spike propagation in the stochastic Hodgkin-Huxley models. *Biol Cybern* **66**, 19–25 (1991)
19. Iannella, N., Tanaka, S., Tuckwell, H.: Firing properties of a stochastic PDE model of a rat sensory cortex layer 2/3 pyramidal cell. *Math Biosci* **188**, 117–132 (2004)
20. Kallianpur, G., Xiong, J.: Diffusion approximation of nuclear spacevalued stochastic differential equations driven by Poisson random measures. *Annals of Appl Prob* **5**, 493–517 (1995)
21. Koch, C.: *Biophysics of Computation: Information processing in single neurons*. Oxford University Press, Oxford UK (1999)
22. Komendantov, A., Tasker, J., Trayanova, N.: Somato-dendritic mechanisms underlying the electrophysiological properties of hypothalamic magnocellular neuroendocrine cells: A multicompartmental model study. *J Comput Neurosci* **23**, 143–168 (2007)
23. Levitan, I., Kaczmarek, L.: *Neuromodulation*. Oxford University Press, Oxford UK (1987)
24. Lindner, B., Garcia-Ojalvo, J., Neiman, A., L, S.G.: Effects of noise in excitable systems. *Phys Rep* **392**, 321–424 (2004)
25. Llinas, R.: The intrinsic electrophysiological properties of mammalian neurons: insights into central nervous system function. *Science* **242**, 1654–1664 (1988)
26. Mainen, Z., Joerges, J., Huguenard, J., Sejnowski, T.: A model of spike initiation in neocortical pyramidal neurons. *Neuron* **15**, 1427–1439 (1995)
27. Markram, H., Toledo-Rodriguez, M., Wang, Y., Gupta, A., Silberberg, G., Wu, C.: Interneurons of the neocortical inhibitory system. *Nat Rev Neurosci* **5**, 793–807 (2004)
28. McCormick, D., Huguenard, J.: A model of the electrophysiological properties of thalamocortical relay neurons. *J Neurophysiol* **68**, 1384–1400 (1992)
29. Megías, M., Emri, Z., Freund, T., Gulyás, A.: Total number and distribution of inhibitory and excitatory synapses on hippocampal CA1 pyramidal cells. *Neurosci* **102**, 527–540 (2001)
30. Meir, A., Ginsburg, S., Butkevich, A., Kachalsky, S., Kaiserman, I., Ahdut, R., Demirgoren, S., Rahamimoff, R.: Ion channels in presynaptic nerve terminals and control of transmitter release. *Physiol Rev* **79**, 1020–1088 (1999)
31. Rhodes, P., Llinas, R.: A model of thalamocortical relay cells. *J Physiol* **565**, 765–781 (2005)
32. Roy, B., Smith, D.: Analysis of the exponential decay model of the neuron showing frequency threshold effects. *Bull Math Biophys* **31**, 341–357 (1969)
33. Sholl, D.: *The organization of the cerebral cortex*. Methuen, London UK (1956)
34. Skaugen, E., Walloe, L.: Firing behaviour in a stochastic nerve membrane model based upon the Hodgkin-Huxley equations. *Acta Physiol Scand* **107**, 343–363 (1979)
35. Spruston, N.: Pyramidal neurons: dendritic structure and synaptic integration. *Nat Rev Neurosci* **9**, 206–221 (2008)
36. Traub, R.: Motoneurons of different geometry and the size principle. *Biol Cybern* **25**, 163–175 (1977)
37. Traub, R.: Neocortical pyramidal cells: a model with dendritic calcium conductance reproduces repetitive firing and epileptic behavior. *Brain Res* **173**, 243–257 (1979)
38. Tuckwell, H.: Synaptic transmission in a model for stochastic neural activity. *J Theor Biol* **77**, 65–81 (1979)

39. Tuckwell, H.: Poisson Processes in Biology. In: Stochastic Nonlinear Systems, pp. 162–172. Springer, Berlin (1981)
40. Tuckwell, H.: Stochastic equations for nerve membrane potential. *J Theoret Neurobiol* **5**, 87–99 (1986)
41. Tuckwell, H.: Introduction to theoretical neurobiology, Vol.1: Linear cable theory and dendritic structure. Cambridge Univ. Press, Cambridge (1988)
42. Tuckwell, H.: Introduction to theoretical neurobiology, Vol.2: Nonlinear and stochastic theories. Cambridge Univ. Press, Cambridge (1988)
43. Tuckwell, H.: Stochastic Processes in the Neurosciences. SIAM, Philadelphia (1989)
44. Tuckwell, H.: Spatial neuron model with two-parameter Ornstein-Uhlenbeck input current. *Physica A* **368**, 495–510 (2006)
45. Tuckwell, H.: Analytical and simulation results for the stochastic spatial FitzHugh-Nagumo neuron. *Neural Computation* **20**, 3003–3035 (2008)
46. Tuckwell, H., Jost, J.: The effects of various spatial distributions of weak noise on rhythmic spiking. *J Comp Neurosci* DOI pp. 10.1007/s10,827–010–0260–5 (2010)
47. Tuckwell, H., Jost, J.: Weak noise in neurons may powerfully inhibit the generation of repetitive spiking but not its propagation. *PLoS Comp Biol* **6**, e1000,794 (2010)
48. Tuckwell, H., Jost, J., Gutkin, B.: Inhibition and modulation of rhythmic neuronal spiking by noise. *Phys Rev E* **80**, 031,907 (2009)
49. Tuckwell, H., Walsh, J.: Random currents through nerve membranes. *Biol Cybern* **49**, 99–110 (1983)
50. Tuckwell, H., Wan, F., Rospars, J.: A spatial stochastic neuronal model with Ornstein-Uhlenbeck input current. *Biol. Cybern.* **86**, 137–145 (2002)
51. Tuckwell, H., Wan, F., Wong, Y.S.: The interspike interval of a cable model neuron with white noise input. *Biol Cybern* **49**, 155–167 (1984)
52. Watts, J., Thomson, A.: Excitatory and inhibitory connections show selectivity in the neocortex. *J. Physiol* **562.1**, 89–97 (2005)
53. Y, S., Hasenstaub, A., Badoual, M., Bal, T., McCormick, D.: Barrages of synaptic activity control the gain and sensitivity of cortical neurons. *J Neurosci* **23**, 10,388–10,401 (2003)
54. Zhang, X., You, G., Chen, T., Feng, J.: Maximum likelihood decoding of neuronal inputs from an interspike interval distribution. *Neural Comput* **21**, 1–27 (2009)